One-way quantum computing in superconducting circuits

F. Albarrán-Arriagada,[1,*] G. Alvarado Barrios,[1] M. Sanz,[2] G. Romero,[1] L. Lamata,[2] J. C. Retamal,[1,3] and E. Solano[2,4,5]

[1]*Departamento de Física, Universidad de Santiago de Chile (USACH), Avenida Ecuador 3493, 9170124, Santiago, Chile*
[2]*Department of Physical Chemistry, University of the Basque Country UPV/EHU, Apartado 644, 48080 Bilbao, Spain*
[3]*Center for the Development of Nanoscience and Nanotechnology 9170124, Estación Central, Santiago, Chile*
[4]*IKERBASQUE, Basque Foundation for Science, Maria Diaz de Haro 3, 48013 Bilbao, Spain*
[5]*Department of Physics, Shanghai University, 200444 Shanghai, China*

We propose a method for the implementation of one-way quantum computing in superconducting circuits. Measurement-based quantum computing is a universal quantum computation paradigm in which an initial cluster state provides the quantum resource, while the iteration of sequential measurements and local rotations encodes the quantum algorithm. Up to now, technical constraints have limited a scalable approach to this quantum computing alternative. The initial cluster state can be generated with available controlled-phase gates, while the quantum algorithm makes use of high-fidelity readout and coherent feedforward. With current technology, we estimate that quantum algorithms with above 20 qubits may be implemented in the path toward quantum supremacy. Moreover, we propose an alternative initial state with properties of maximal persistence and maximal connectedness, reducing the required resources of one-way quantum computing protocols.

I. INTRODUCTION

Quantum computation has experienced a fast and remarkable development in recent decades [1–10]. This progress is based on the astonishing development of quantum platforms that currently allow for the manipulation and control of highly coherent qubits. There are several equivalent quantum computing paradigms for the implementation of a quantum algorithm. The quantum circuit or gate-based approach, which makes use of single- and two-qubit gates for this implementation, is currently the standard one. One-way quantum computing, also known as measurement-based quantum computation [11–13], is an alternative universal quantum computing paradigm, in which a particular kind of entangled multiparticle state, namely the cluster state, constitutes the initial quantum resource. Then, the algorithm is encoded through a sequence of single-qubit readouts and feedforward rotations based on the outcome of these measurements. Cluster states show two relevant properties, namely, persistence of entanglement after single-qubit projective measurements and maximal pairwise connectedness between qubits of the multipartite system. The first property refers to the minimal number of qubits that must be measured such that the resulting state is separable. Cluster states have a persistence of $\lfloor N/2 \rfloor$ [14]. The second property means that any pair of qubits can be projected onto a Bell state by appropriate local measurements on the rest of the qubits.

One-way quantum computing has been experimentally demonstrated in quantum photonics for small systems [15–17]. However, these implementations are not scalable because of the nondeterministic generation of the cluster state. Nonetheless, there have been theoretical proposals to avoid these issues

[18]. On the other hand, the proposals in trapped ions [19,20] allow for scalable generation of cluster states, but the implementation of quantum algorithms is limited by the long qubit readout times. Indeed, measurements based on electron shelving ($\sim$10 ms [21]) take longer than the average coherence time of the ions ($\sim$3 ms [22]), which is a handicap for large protocols.

There has been remarkable progress in technologies based on superconducting circuits in recent years [23–27], which has allowed the scalable generation of large entangled states [8,28,29]. Additionally, fast feedforward protocols have also been developed recently [30–32]. Although theoretical proposals for the generation of cluster states in superconducting circuits have been made over a decade ago [33–36], the state of the technology at the time made the implementation of these approaches difficult.

In this work, we propose an experimentally feasible implementation of one-way quantum computing in superconducting circuits. First, we show how to efficiently generate two-dimensional (2D) cluster states by using high-fidelity controlled-Z gates, which are standard in this platform. We study the implementation of feedforward protocols and apply this to the generation of a universal C-NOT gate. Finally, we propose an alternative initial state with maximal persistence which can be straightforwardly generated in superconducting circuits. We show that the implementation of quantum algorithms with this multipartite state requires 25% fewer ancillary qubits and measurements than with cluster states, substantially improving the involved scalability aspects.

II. CLUSTER STATE AND C-NOT GATE GENERATION

First, we propose a digital generation of cluster states, the quantum resource for measurement-based quantum com-

*francisco.albarran@usach.cl

puting. Our protocol is based on the controlled-Z gate (C^z) implemented by Barends *et. al.* [7,37] in Xmon qubits [38]. The Xmon is a tunable nonlinear system, which allows us to define qubit states $|1\rangle$ and $|0\rangle$ in its ground and first excited states, respectively, and an auxiliary state $|a\rangle$ in the second excited state. As described in Ref. [7], in the implementation of the C^z gate the Xmon qubits are capacitively coupled. Tuning the energy gap between the states $\{|0\rangle,|a\rangle\}$ of the first Xmon to match the energy gap between the states $\{|1\rangle,|0\rangle\}$ of the adjacent Xmon it is possible to activate an exchange evolution between them that is given by $U = e^{-\frac{i}{\hbar}Vt}$, with $V = \hbar g(|0\rangle|0\rangle\langle 1|\langle a| + \text{H.c.})$. The C^z gate is realized for $gt = \pi$, that allows us to implement the conditional change $|0\rangle|0\rangle \rightarrow -|0\rangle|0\rangle$.

The cluster state $|C_N\rangle$ of a lattice of N particles is written as $|C_N\rangle = \mathcal{U}\bigotimes_j |+_j\rangle$, where the operator $\mathcal{U}$ is given by the time evolution operator $\mathcal{U} = e^{-iH\pi}$ [39], with

$$H = \sum_{\langle j,k\rangle, k>j} \left(\frac{1+\sigma_j^z}{2}\right)\left(\frac{1-\sigma_k^z}{2}\right), \quad |+_j\rangle = \frac{|0_j\rangle + |1_j\rangle}{\sqrt{2}},$$

(1)

with $|0_j\rangle$ and $|1_j\rangle$ being the eigenstates of σ_j^z with eigenvalues 1 and -1 respectively, $\langle j,k\rangle$ denotes that the sites j and k are nearest neighbors. The effect of $\mathcal{U}$ over each pair of adjacent qubits is a controlled-Z gate, with $|0_j 1_k\rangle \rightarrow -|0_j 1_k\rangle$, where j is the control and k the target qubit. Therefore, we can write a cluster state as [39]

$$|C_N\rangle = \frac{1}{2^{N/2}} \bigotimes_{\ell=1}^{N-1} \left[|0_\ell\rangle \left(\prod_j \sigma_{\langle \ell_j\rangle}^z\right) + |1_\ell\rangle \right],$$

(2)

where $\langle \ell_j\rangle$ refers to the jth nearest neighbor of ℓ.

This effect can be simulated using a combination of C^z gates over Xmon qubits. As described in Ref. [7], this gate changes the state $|0_j\rangle|0_K\rangle$ into $-|0_j\rangle|0_K\rangle$, acting as the identity on the remaining states, where $|0\rangle$ and $|1\rangle$ stand for the excited and ground states of the Xmon qubit, respectively. Then, the gate C^z performs a $-\sigma_z$ on the target when the control qubit is in the state $|0\rangle$. This differs slightly from the action of the $\mathcal{U}$ gate that activates a σ_z gate on the target. Therefore, to obtain the state given by Eq. (2), we change the initial state as follows: The sites that act as a control for an even number of gates are initialized in the $|+\rangle$ state, and the sites that act as a control for odd number of gates are initialized in the state $|-\rangle = (-|0\rangle + |1\rangle)/\sqrt{2}$. In Fig. 1, we show the initial state for the square lattice.

As an example, we write the cluster state for a $h \times l$ square lattice. For this case, we define a convenient notation and denote each point in the lattice by a vector $\vec{p} = (j,k)$, where j and k denote the jth column and kth row respectively. In Fig. 1, the site $(1,1)$ represent the left lower corner. We also define $\hat{\imath} = (1,0)$ and $\hat{\jmath} = (0,1)$, and obtain

$$|C_N^{hl}\rangle = \left[\prod_{\vec{p}\in\{\mathcal{L}+\mathcal{L}_x\}} \mathcal{C}_{(\vec{p},\vec{p}+\hat{\imath})}^z\right]\left[\prod_{\vec{p}\in\{\mathcal{L}+\mathcal{L}_y\}} \mathcal{C}_{(\vec{p}_x,\vec{p}_x+\hat{\jmath})}^z\right]$$
$$\times \left[\bigotimes_{\vec{p}\in\mathcal{L}} |+_{\vec{p}}\rangle\right]\left[\bigotimes_{\vec{p}\in\mathcal{L}_x} |-_{\vec{p}}\rangle\right]\left[\bigotimes_{\vec{p}\in\mathcal{L}_y} |-_{\vec{p}}\rangle\right] \otimes |+_{(h,l)}\rangle,$$
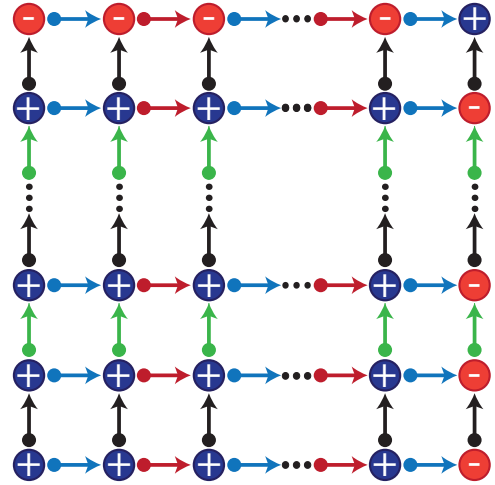
(3)

FIG. 1. Square lattice for the generation of a cluster state. Each link between sites indicates a $\mathcal{C}_z$ gate, where the dot indicates the control site and the arrow the target site. The color of the links indicates the gates that can be performed simultaneously; to perform the blue, red, black, and green interactions it requires four steps overall. The sites marked with "+" are initialized in the $|+\rangle$ state, an the sites marked with "−" are initialized in the $|-\rangle$ state.

where $\mathcal{L} = \{(j,k)\}$, $\mathcal{L}_x = \{(j,l)\}$, $\mathcal{L}_y = \{h,k\}$, with $j = \{1,2,\ldots,h-1\}$ and $k = \{1,2,\ldots,l-1\}$. In Fig. 1, $\mathcal{L}$ contains all blue points, except the right upper corner, $\mathcal{L}_x$ contains the red points in the right boundary, and $\mathcal{L}_y$ contains the red points in the upper boundary.

The effect of $C_{j,k}^z$ can be thought of as a time evolution given by $e^{-i\bar{H}_{j,k}\pi}$, with $\bar{H}_{j,k} = (1+\sigma_j^z)(1+\sigma_k^z)/4$, and defining $\mathcal{H} = \sum_{\langle j,k\rangle} \bar{H}_{j,k}$, we rewrite Eq. (3) as

$$\left|C_N^{hl}\right\rangle = e^{-i\mathcal{H}\pi}\left[\bigotimes_{\vec{p}\in\mathcal{L}} |+_{\vec{p}}\rangle \bigotimes_{\vec{p}\in\mathcal{L}_x} |-_{\vec{p}}\rangle \bigotimes_{\vec{p}\in\mathcal{L}_y} |-_{\vec{p}}\rangle\right] \otimes |+_{(h,l)}\rangle.$$

(4)

Although all components $\bar{H}_{j,k}$ of the Hamiltonian commute, the physical implementation of $\mathcal{C}^z$ prohibits the simultaneous realization of gates that share qubits [37]. Then, we separate the Hamiltonian $\mathcal{H}$ in Eq. (4) into terms corresponding to the gates that can be performed at the same time and write $\mathcal{H} = \mathcal{H}_1^x + \mathcal{H}_2^x + \mathcal{H}_1^y + \mathcal{H}_2^y$, where

$$\mathcal{H}_\ell^x = \sum_{\vec{p}\in A_\ell^x} \left(1+\sigma_{\vec{p}}^z\right)\left(1+\sigma_{\vec{p}+\hat{\imath}}^z\right),$$
$$\mathcal{H}_\ell^y = \sum_{\vec{p}\in A_\ell^y} \left(1+\sigma_{\vec{p}}^z\right)\left(1+\sigma_{\vec{p}+\hat{\jmath}}^z\right),$$

(5)

with $\ell = \{1,2\}$. A_ℓ^x and A_ℓ^y correspond to the set of points of the form $(2n_x + \ell, k)$ and $(j, 2n_y + \ell)$, respectively, where $k = \{1,2,\ldots,l\}$, $j = \{1,2,\ldots,h\}$, $n_x = \{0,1,\ldots,h/2 - 2\}$, and $n_y = \{0,1,\ldots,l/2 - 2\}$. Therefore, we can simulate the evolution $e^{-i\mathcal{H}\pi}$ in four steps. In Fig. (1), the controlled-Z gates that produce the evolutions $e^{-i\mathcal{H}_1^x\pi}$, $e^{-i\mathcal{H}_2^x\pi}$, $e^{-i\mathcal{H}_1^y\pi}$, and $e^{-i\mathcal{H}_2^y\pi}$ are represented by blue, red, black, and green links respectively. As all Hamiltonians $\mathcal{H}_j^\alpha$ commute, no digital error is committed.
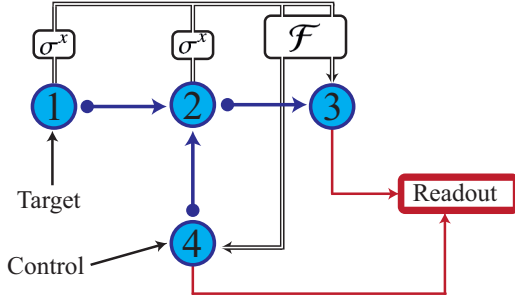
FIG. 2. Schematic protocol for the C-NOT gate. Qubits 1 and 4 are the target and control qubits, respectively, and the sites 2 and 3 are initialized in the states $|-\rangle$ and $|+\rangle$, respectively. The arrows indicate the order in which the interaction is considered, where the circles are attached to the control qubits for the CZ gate, and the arrow end to the target. Finally we measure qubits 1 and 2, and with this information we perform a feedback over the readout qubits (3 and 4).

Finally, the elapsed time reported for the $\mathcal{C}^z$ gate is around $t_{CZ} \approx 0.05\,[\mu s]$ with average fidelity 99.5% [7], and then for a 4×4 lattice, the protocol can generate a cluster state with average fidelity of 88% in $0.2\,[\mu s]$.

Consider now, as a specific example of a two-qubit gate, the implementation of the C-NOT. Pedagogically, we will use the previous developed gate as in Ref. [11]. Let us use the protocol of Fig. 2, where qubit 1 is the target, qubit 4 is the control, and the sites 2 and 3 are initialized in the states $|-\rangle$ and $|+\rangle$, respectively. The initial state reads

$$|\Phi_o\rangle = |i_1\rangle_z|j_4\rangle_z|1_2\rangle_x|0_3\rangle_x, \tag{6}$$

where the subindexes z and x indicate that we use the eigenbasis of σ^z and σ^x, respectively. Now, we perform the entangling gate $U = \mathcal{C}^z_{(1,2)}\mathcal{C}^z_{(4,2)}\mathcal{C}^z_{(2,3)}$, as represented by the arrow links in Fig. 2, thus generating the initial resource state for the implementation of the C-NOT gate. Afterward, we measure the sites 1 and 2 in the σ^x basis with a respective feedforward over the sites 3 and 4, obtaining the state

$$|\Phi_m\rangle = \mathcal{F}_{3,4}|l_1\rangle_z|m_2\rangle_z|(i \oplus j)_3\rangle_z|j_4\rangle_z, \tag{7}$$

where $\mathcal{F}_{3,4} = (\sigma^z_3\sigma^z_4)^l(\sigma^x_3)^m$ is the feedforward operator and l and m are the output of the measurement of qubits 1 and 2, respectively. The reported elapsed time for the measurement and digital feedforward process is approximately $2\,[\mu s]$ [40], with an error of 1% for the measurement and 1% for the feedforward process. Then, a rough estimation of the fidelity of this protocol yields 95%, in a time smaller than $5\,[\mu s]$, which is significantly smaller than the average Xmon coherence time [38]. The elapsed times and fidelity we mentioned before correspond to an effective estimation taking into consideration gate sequences, feedback delays, and readout times which have been experimentally reported [40]. Based on our estimations, we expect that, with current technology, it could be possible to implement quantum algorithms of up to five two-qubit gates and requiring approximately 20 qubits with a fidelity lower bounded roughly by 80%.
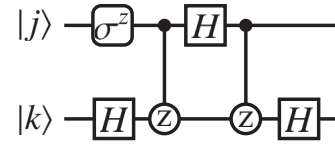

FIG. 3. Circuit to construct the $U^{\text{Bell}}_{j,k}$ gate given in Eq. (8).

III. ALTERNATIVE ENTANGLING GATE

One of the limitations faced by measurement-based quantum computing is the number of qubits required for the implementation of quantum algorithms. In what follows, we propose an alternative entangling gate, which we have termed U^{Bell}, and show that it reduces the number of qubits needed for one-way quantum computing. In addition, this gate enables the generation of maximal persistence states, allowing, for instance, the implementation of an efficient C-NOT protocol for one-way quantum computing. We summarize the action of this gate as follows:

$$
\begin{aligned}
U^{\text{Bell}}_{j,k}|0_j0_k\rangle &= \sqrt{\frac{1}{2}}(|0_j0_k\rangle + |1_j1_k\rangle), \\
U^{\text{Bell}}_{j,k}|0_j1_k\rangle &= \sqrt{\frac{1}{2}}(|0_j1_k\rangle + |1_j0_k\rangle), \\
U^{\text{Bell}}_{j,k}|1_j0_k\rangle &= \sqrt{\frac{1}{2}}(|1_j0_k\rangle - |0_j1_k\rangle), \\
U^{\text{Bell}}_{j,k}|1_j1_k\rangle &= \sqrt{\frac{1}{2}}(|1_j1_k\rangle - |0_j0_k\rangle).
\end{aligned}
\tag{8}
$$

Within the Xmon architecture discussed in the previous section, this gate could be implemented using the circuit shown in Fig. 3, which involves one- and two-qubit gates among adjacent Xmons. However, it is worth mentioning that the $U^{\text{Bell}}_{j,k}$ gate could be implemented as the time evolution $U^{\text{Bell}}_{j,k} = e^{-\frac{i}{\hbar}H^{x,y}_{j,k}\tau}$, with the Hamiltonian $H^{x,y}_{j,k} = \hbar\xi(J_1\sigma^x_j\sigma^x_k - J_2\sigma^y_j\sigma^x_k)$, where $J_1 = 5/4$, $J_2 = 1$, and $\xi\tau = \pi$. It is not clear whether it is possible to implement this Hamiltonian in the Xmon qubit architecture. Nevertheless, the Hamiltonian $H^{x,y}_{j,k}$ can be implemented using a chain of qubit-cavity systems in the ultrastrong coupling regime, with variable coupling, as shown in a recent theoretical work [41], which is summarized in the appendix.

In what follows, we show that by using the $U^{\text{Bell}}_{j,k}$ entangling gate it is possible to generate an entangled multiparticle state that plays a similar role as the cluster state as a resource for one-way quantum computing. This state allows us to implement a C-NOT gate that only requires three qubits and one measurement, which is an improvement over the four qubits and two measurements needed for the usual cluster state generated by the $\mathcal{C}^z_{(j,k)}$ gate, as was shown in the previous section. The protocol is summarized in Fig. 4. The sites 1, 2, and 3 correspond to target input, target output, and control input qubit, respectively. The initial state is given by

$$|\Psi_o\rangle = |i_1\rangle_z|0_2\rangle_z|j_3\rangle_z. \tag{9}$$

Now, we perform the $U^{\text{Bell}}_{1,2}$ gate which leads to

$$|\Psi_1\rangle = \sqrt{\frac{1}{2}}[|i_1\rangle_z|0_2\rangle_z + (-1)^i|(i \oplus 1)_1\rangle_z|1_2\rangle_z]|j_3\rangle_z. \tag{10}$$
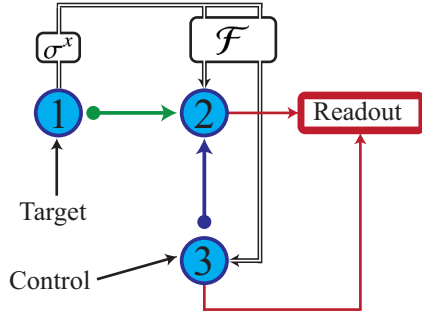
FIG. 4. Schematic protocol for our efficient C-NOT gate, where qubits 1 and 3 are the target and control, respectively, and site 2 is initialized in the state $|0\rangle$. The blue arrow refers to the gate $\mathcal{C}_{3,2}$ and the green arrow for the gate $U^{\text{Bell}}_{1,2}$. Finally, we measure qubit 1, and with this information we perform a feedback over the nonmeasured qubits (2 and 3).

Next, we do the $\mathcal{C}^z_{3,2}$ gate and obtain

$$|\Psi_2\rangle = \sqrt{\frac{1}{2}}[(-1)^{j+1}|i_1\rangle_z|0_2\rangle_z + (-1)^i|(i \oplus 1)_1\rangle_z|1_2\rangle_z]|j_3\rangle_z.$$
(11)

This state will be the resource that plays a similar role as the cluster state, with the improvement that it only requires a single measurement to implement a C-NOT gate, as will be shown as follows.

Measuring σ^x in qubit 1 yields

$$|\Psi_3\rangle = \sqrt{\frac{1}{2}}[(-1)^{j+1+i\cdot s}|s_1\rangle_x|0_2\rangle_z + (-1)^{i+i\cdot s+s}|s_1\rangle_x|1_2\rangle_z] \times |j_3\rangle_z,$$
(12)

where $s \in \{0,1\}$ is the outcome of the σ^x measurement. Then, we perform a Hadamard gate over qubit 2, obtaining

$$|\Psi_4\rangle = \frac{(-1)^{i\cdot s}}{2}|s_1\rangle_x\{[(-1)^{j+1} + (-1)^{i+s}]|0_2\rangle_z \\ + [(-1)^{j+1} - (-1)^{i+s}]|1_2\rangle_z\}|j_3\rangle_z.$$
(13)

If $s = 0$, we obtain $|\Psi_4\rangle = (-1)^{j+1}|0_1\rangle_x|j_3\rangle_z|(i \oplus j \oplus 1)_2\rangle_z$, and if $s = 1$, we obtain $|\Psi_4\rangle = (-1)^{i+j+1}|1_1\rangle_x|j_3\rangle_z|(i \oplus j)_2\rangle_z$. Then, when $s = 0$ we need to activate the operator $-\sigma^x_2\sigma^z_3$, and when $s = 1$ we need to activate the operator $-\sigma^z_2$ in order to recover the usual C-NOT gate, where qubit 2 becomes the target qubit. Therefore, using feedforward operator $\mathcal{F} = (-\sigma^x_2\sigma^z_3)^{s+1}(-\sigma^z_2)^s$, we have $\mathcal{F}|\Psi_4\rangle = |s_1\rangle_x|j_3\rangle_z|(i \oplus j)_2\rangle_z$. As $U^{\text{Bell}}_{1,2}$ and $\mathcal{C}^z_{3,2}$ do not commute, the order in which the gates are applied is important.

As is shown in Fig. 3, the gate U^{Bell} can be constructed using three Hadamard gates, two CZ gates, and a σ_z gate. A rough estimation of the fidelity yields 98.8% and requires a time of less than 0.3 [μs]. As we have seen, the C-NOT requires one U^{Bell} and one C^z gate. It can be done with a fidelity around 96.5% in a time 2.5 [μs]. Therefore, the implementation of quantum algorithms using this protocol requires 25% less ancillary qubits, substantially improving scalability. For example, an array of 16 qubits allows for four C-NOT gates with the standard protocol, whereas it is possible to implement five C-NOT gates with our protocol. Furthermore,

since the C-NOT and arbitrary qubit rotations form a universal set [42], we can expect that the reduction in necessary resources enabled by the U^{Bell} entangling gate will extend to more complex quantum algorithms since any quantum algorithm can be decomposed into C-NOT gates and single-qubit rotations.

Also, the U^{Bell} operator allows the generation of maximally persistent and maximally connected (MPMC) states. We start with the initial state $|\phi_o\rangle = \otimes^N_{\ell=1}|0_\ell\rangle$, to which we apply the gate $U^{\text{Bell}}_{j,k}$ simultaneously over qubit pairs in the sites $(2\ell - 1, 2\ell)$, followed by the same operation on qubit pairs in sites $(2\ell, 2\ell + 1)$, obtaining

$$|\mathfrak{C}_N\rangle = \left[\prod_{\ell=1}^{N/2-1} U^{\text{Bell}}_{2\ell,2\ell+1}\right]\left[\prod_{\ell=1}^{N/2} U^{\text{Bell}}_{2\ell-1,2\ell}\right]\bigotimes_{\ell=1}^N |0_\ell\rangle$$

$$= \frac{1}{2^{N/4}}\left[\prod_{\ell=1}^{N/2-1} U^{\text{Bell}}_{2\ell,2\ell+1}\right]$$

$$\times \bigotimes_{\ell=1}^{N/2}[|0_{2\ell-1}\rangle|0_{2\ell}\rangle + |1_{2\ell-1}\rangle|1_{2\ell}\rangle].$$
(14)

As an example, for three and four particles, we have the state

$$|\mathfrak{C}_3\rangle = U^{\text{Bell}}_{2,3}|\mathfrak{C}_2\rangle|0\rangle = \frac{1}{\sqrt{2}}(|\mathfrak{C}_2\rangle|0\rangle + |\mathfrak{C}^\perp_2\rangle|1\rangle),$$
(15)

where $|\mathfrak{C}_2\rangle = (|0\rangle|0\rangle + |1\rangle|1\rangle)/\sqrt{2}$ and $|\mathfrak{C}^\perp_2\rangle = (|0\rangle|1\rangle - |1\rangle|0\rangle)/\sqrt{2}$ are orthogonal cluster states of two particles. And we also have

$$|\mathfrak{C}_4\rangle = U^{\text{Bell}}_{2,3}|\mathfrak{C}_2\rangle|\mathfrak{C}_2\rangle = \frac{1}{\sqrt{2}}(|\mathfrak{C}_3\rangle|0\rangle + |\mathfrak{C}^\perp_3\rangle|1\rangle),$$
(16)

where $|\mathfrak{C}^\perp_3\rangle = (|\mathfrak{C}_2\rangle|1\rangle + |\mathfrak{C}^\perp_2\rangle|0\rangle)/\sqrt{2}$, is a MPMC state of three particles orthogonal to $|\mathfrak{C}_3\rangle$. Then, if $|\mathfrak{C}_{N-2}\rangle = (|\mathfrak{C}_{N-3}\rangle|0\rangle + |\mathfrak{C}^\perp_{N-3}\rangle|1\rangle)/\sqrt{2}$, we have

$$|\mathfrak{C}_N\rangle = U^{\text{Bell}}_{N-2,N-1}|\mathfrak{C}_{N-2}\rangle|\mathfrak{C}_2\rangle$$

$$= \frac{1}{\sqrt{2}}\left[\frac{1}{\sqrt{2}}(|\mathfrak{C}_{N-2}\rangle|0\rangle + |\mathfrak{C}^\perp_{N-2}\rangle|1\rangle)|0\rangle\right.$$

$$\left. + \frac{1}{\sqrt{2}}(|\mathfrak{C}_{N-2}\rangle|1\rangle + |\mathfrak{C}^\perp_{N-2}\rangle|0\rangle)|1\rangle\right]$$

$$= \frac{1}{\sqrt{2}}(|\mathfrak{C}_{N-1}\rangle|0\rangle + |\mathfrak{C}^\perp_{N-1}\rangle|1\rangle),$$
(17)

where $|\mathfrak{C}_{N-1}\rangle = (|\mathfrak{C}_{N-2}\rangle|0\rangle + |\mathfrak{C}^\perp_{N-2}\rangle|1\rangle)/\sqrt{2}$ and $|\mathfrak{C}^\perp_{N-1}\rangle = (|\mathfrak{C}_{N-2}\rangle|1\rangle + |\mathfrak{C}^\perp_{N-2}\rangle|0\rangle)/\sqrt{2}$ are orthogonal MPMC states. It is straightforward to show that any two qubits can be projected into a Bell state by measuring all the remaining qubits in the σ^z basis, which means that the $|\mathfrak{C}_N\rangle$ are maximally connected. Now, to prove maximal entanglement persistence for these states, we proceed as follows. Suppose that the state $|\mathfrak{C}_{N-1}\rangle$ has a minimal product state decomposition (MPSD) of r terms and, therefore, an entanglement persistence of $\mathcal{P} = \log_2(r)$. As $|\mathfrak{C}^\perp_{N-1}\rangle$ is equal to $|\mathfrak{C}_{N-1}\rangle$ under local rotations, then $|\mathfrak{C}^\perp_{N-1}\rangle$ also has a MPSD of r terms. Thus, we see that the state $|\mathfrak{C}_N\rangle$ in Eq. (17) is a decomposition in $2r$ terms. Thus, $|\mathfrak{C}_N\rangle$ reads

$$|\mathfrak{C}_N\rangle = \sum_{k=1}^{2r}\left(\lambda_k \bigotimes_{\ell=1}^N |\alpha^{(k)}_\ell\rangle\right),$$
(18)

where $|\alpha_\ell^{(k)}\rangle$ is the state of particle ℓ and $\sum_{k=1}^{2r} \lambda_k^2 = 1$. If Eq. (18) is not a MPSD, we can write

$$|\mathfrak{C}_N\rangle = \sum_{k=1}^{2r-2} \left(\lambda_k \bigotimes_{\ell=1}^{N} |\alpha_\ell\rangle\right) + \bar{\lambda}|\varphi\rangle\left(\beta_0|\alpha_a^{2r-1}\rangle + \beta_1|\alpha_a^{2r}\rangle\right),$$

(19)

where $\bar{\lambda}^2 = \lambda_{2r-1}^2 + \lambda_{2r}^2$, $\beta_0 = \lambda_{2r-1}/\bar{\lambda}$, $\beta_1 = \lambda_{2r}/\bar{\lambda}$, and $|\varphi\rangle$ is a state involving every other particle except particle a. This reduction is not possible because $|\mathfrak{C}_{N-1}\rangle$ and $|\mathfrak{C}_{N-1}^\perp\rangle$ do not share any terms. Then, $a \neq N$ and, as $|\mathfrak{C}_{N-1}\rangle$ and $|\mathfrak{C}_{N-1}^\perp\rangle$ are in their MPSD, we conclude that $a \neq \{1, 2, \ldots N-1\}$. Therefore, Eq. (18) is the MPSD with $2r$ terms and persistence $\mathcal{P} = \log_2(2r)$. As the MPSD of $|\mathfrak{C}_2\rangle$ is $r = 2$, for $|\mathfrak{C}_N\rangle$ it is $r = 2^{N-1}$, and its persistence $\mathcal{P} = N-1$ is maximal.

IV. CONCLUSIONS

We have shown that current technology in superconducting circuits enables the consideration of measurement-based quantum computing algorithms, avoiding operational time problems which affect scalability in other quantum computing platforms. Initially, we generated a two-dimensional $N \times N$ cluster state by making use of $2N(N-1)$ experimentally available controlled-phase gates. A quantum algorithm is generated by using single-qubit measurements and coherent feedforward. In particular, we applied this approach to the case $N = 2$ to implement the universal C-NOT gate with an estimated fidelity lower bounded by 95%. Rough calculations, based on reported experimental parameters, allow us to estimate that we can perform algorithms above 20 qubits. Additionally, we propose an alternative and experimentally feasible entangling gate, which reduces the number of required qubits in a 25% per implemented C-NOT gate. This fact reduces the number of measurements and feedforward processes, which improves the fidelity of the protocol. Therefore, the perspective toward scalability and quantum supremacy is open with steady current improvements in midsized superconducting quantum platforms.

APPENDIX: POSSIBLE IMPLEMENTATION OF U^{Bell} GATE

A recent theoretical work [41] has proposed a system in which the U^{Bell} gate could be implemented. This system consists of a chain of qubit-cavity systems in the ultrastrong coupling regime named quantum Rabi systems (QRSs). In

this proposal, each QRS is coupled to its nearest-neighbor trough grounded superconducting quantum interference devices (SQUIDs). This chain is described by

$$
\begin{aligned}
H = \sum_{\ell=1}^{N} & \left[H_\ell^{\text{QRS}} + \left(P_\ell^{\ell,\ell+1} + P_\ell^{\ell-1,\ell}\right)(a_\ell^\dagger + a_\ell)^2\right] \\
& - \sum_{\ell=1}^{N-1} \left[2\sqrt{P_\ell^{\ell,\ell+1} P_{\ell+1}^{\ell,\ell+1}}(a_\ell^\dagger + a_\ell)(a_{\ell+1}^\dagger + a_{\ell+1})\right] \\
& + \sum_{\ell=1}^{N} \left[\left(Q_\ell^{\ell,\ell+1}\bar{\Phi}_{\ell,\ell+1}(t) + Q_\ell^{\ell,\ell-1}\bar{\Phi}_{\ell,\ell-1}(t)\right)(a_\ell^\dagger + a_\ell)^2\right] \\
& - \sum_{\ell=1}^{N-1} \left[2\sqrt{Q_\ell^{\ell,\ell+1} Q_{\ell+1}^{\ell,\ell+1}}\bar{\Phi}_{\ell,\ell+1}(t) \right. \\
& \left. \times (a_\ell^\dagger + a_\ell)(a_{\ell+1}^\dagger + a_{\ell+1})\right],
\end{aligned}
$$

(A1)

where $P_\ell^{\ell,\ell+1}$ and $Q_\ell^{\ell,\ell+1}$ are time-independent constants that depend on the characteristics of each site ℓ and coupling between the QRSs ℓ and $\ell+1$, $\bar{\Phi}_{\ell,\ell+1}(t)$ are time-dependent magnetic signals threading the SQUID that couple the sites ℓ and $\ell+1$, and a_ℓ and $a_\ell^\dagger$ are the annihilation and creation operators of the cavity corresponding to the ℓth QRS respectively. Finally H_ℓ^{QRS} is the Hamiltonian of the ℓth QRS given by

$$H_\ell^{\text{QRS}} = \frac{\hbar\omega_\ell^q}{2}\sigma_\ell^z + \hbar\omega_\ell^r a_\ell^\dagger a_\ell + \hbar g_\ell \sigma_\ell^x(a_\ell^\dagger + a_\ell),$$ (A2)

with ω_ℓ^q, ω_ℓ^r, and g_ℓ being the qubit frequency, cavity frequency, and coupling strength belonging to the ℓ site respectively. Also, σ_ℓ^k is the k-Pauli matrix of the qubit in the ℓth QRS. We define the QRS basis by $\{|j\rangle_\ell\}$ by $H_\ell^{\text{QRS}}|j\rangle_\ell = \lambda_j^\ell|j\rangle_\ell$. As the QRS has an anharmonic spectrum, we write the cavity operators in the QRS basis and truncate to the first excited state in order to obtain an effective two-level system per site; also we can consider that $P_\ell^{\ell,\ell+1} = P_\ell$ and $Q_\ell^{\ell,\ell+1} = Q_\ell$ only depend on the site, and the magnetic flux $\bar{\Phi}_{\ell,\ell+1}(t) = \bar{\Phi}(t)$ is the same for all SQUIDs. Then, we obtain for adjacent QRSs

$$
\begin{aligned}
H_{(2)} = \sum_{\ell=1}^{2} & \left[\left(\lambda_0^\ell + 2P_\ell z_{0,0}^\ell\right)|0\rangle_\ell\langle 0| + \left(\lambda_1^\ell + 2P_\ell z_{1,1}^\ell\right)|1\rangle_\ell\langle 1|\right] \\
& -2[\sqrt{P_\ell P_{\ell+1}} + \sqrt{Q_\ell Q_{\ell+1}}\bar{\Phi}(t)]\chi_{0,1}^\ell \chi_{0,1}^{\ell+1}\hat{X}^\ell\hat{X}^{\ell+1} \\
& + \sum_{\ell=1}^{2} 2Q_\ell\bar{\Phi}(t)\left[z_{0,0}^\ell|0\rangle_\ell\langle 0| + z_{1,1}^\ell|1\rangle_\ell\langle 1|\right],
\end{aligned}
$$

(A3)

where $\hat{X}^\ell = |0\rangle_\ell\langle 1| + |1\rangle_\ell\langle 0|$, $z_{j,j}^\ell = {}_\ell\langle j|(a_\ell + a_\ell^\dagger)^2|j\rangle_\ell$ and $\chi_{0,1}^\ell = \chi_{1,0}^\ell = {}_\ell\langle j|(a_\ell + a_\ell^\dagger)|j\rangle_\ell$. As the first line in Eq. (A3) is the diagonal time-independent part of the Hamiltonian, we define the free Hamiltonian by $H_o = \sum_{\ell=1}^{2}[\eta_0^\ell|0\rangle_\ell\langle 0| + \eta_1^\ell|1\rangle_\ell\langle 1|]$, with $\eta_k^\ell = \lambda_k^\ell + 2P_\ell z_{k,k}^\ell$. We can write the Hamiltonian (A3) in the interaction picture with respect to H_o as

$$
\begin{aligned}
H_{(2)}^I = -2\chi_{0,1}^\ell \chi_{0,1}^{\ell+1}(\sqrt{P_\ell P_{\ell+1}} + \sqrt{Q_\ell Q_{\ell+1}}\bar{\Phi}(t)) \\
\times (e^{-i\Delta t}|1\rangle_\ell\langle 0| \otimes |0\rangle_{\ell+1}\langle 1| + e^{-i\delta t}|1\rangle_\ell\langle 0| \otimes |1\rangle_{\ell+1}\langle 0|
\end{aligned}
$$

$$+e^{i\Delta t}|0\rangle_\ell\langle 1|\otimes|1\rangle_{\ell+1}\langle 0|+e^{i\delta t}|0\rangle_\ell\langle 1|\otimes|0\rangle_{\ell+1}\langle 1|)$$

$$+\sum_{\ell=1}^{2}2Q_\ell\bar{\Phi}(t)[z_{0,0}^\ell|0\rangle_\ell\langle 0|+z_{1,1}^\ell|1\rangle_\ell\langle 1|],\qquad (A4)$$

with $\Delta=(\eta_0^\ell-\eta_1^\ell)-(\eta_0^{\ell+1}-\eta_1^{\ell+1})$ and $\delta=(\eta_0^\ell-\eta_1^\ell)+(\eta_0^{\ell+1}-\eta_1^{\ell+1})$. Finally, as $\bar{\Phi}(t)$ is an external magnetic flux, we can choose $\bar{\Phi}(t)=\gamma_+\cos(\Delta t-\pi/2)+\gamma_-\cos(\delta t+\pi/2)$, and defining $\gamma_\pm=(J_1\pm J_2)/(\chi_{0,1}^\ell\chi_{0,1}^{\ell+1}\sqrt{Q_\ell Q_{\ell+1}})$, we can approximate Eq. (A4) using the rotating-wave approxima-

tion (RWA) with respect to the eigenenergies of H_o as

$$H_{(2)}^{\mathrm{I}}\approx i(J_1+J_2)(|0_\ell 1_{\ell+1}\rangle\langle 1_\ell 0_{\ell+1}|-|1_\ell 0_{\ell+1}\rangle\langle 0_\ell 1_{\ell+1}|)$$
$$+i(J_1-J_2)(|1_\ell 1_{\ell+1}\rangle\langle 0_\ell 0_{\ell+1}|-|0_\ell 0_{\ell+1}\rangle\langle 1_\ell 1_{\ell+1}|)$$
$$=J_1\sigma_\ell^x\sigma_{\ell+1}^y-J_2\sigma_\ell^y\sigma_{\ell+1}^x\qquad (A5)$$

for J_1 and J_2 small enough to ensure the RWA. The time evolution of the Hamiltonian (A5) would result in the $U_{\ell,\ell+1}^{\mathrm{Bell}}$ gate, as indicated in the main text.

More details can be found in Ref. [41].

[1] J. M. Taylor, H.-A. Engel, W. Dür, A. Yacoby, C. M. Marcus, P. Zoller, and M. D. Lukin, Nat. Phys. **1**, 177 (2005).

[2] P. Kok, W. J. Munro, K. Nemoto, T. C. Ralph, J. P. Dowling, and G. J. Milburn, Rev. Mod. Phys. **79**, 135 (2007).

[3] R. Raussendorf and J. Harrington, Phys. Rev. Lett. **98**, 190504 (2007).

[4] H. Häffner, C. F. Roos, and R. Blatt, Phys. Rep. **469**, 155 (2008).

[5] T. D. Ladd, F. Jelezko, R. Laflamme, Y. Nakamura, C. Monroe, and J. L. O'Brien, Nature (London) **464**, 45 (2010).

[6] M. Saffman, T. G. Walker, and K. Mølmer, Rev. Mod. Phys. **82**, 2313 (2010).

[7] R. Barends, J. Kelly, A. Megrant, A. Veitia, D. Sank, E. Jeffrey, T. C. White, J. Mutus, A. G. Fowler, B. Campbell *et al.*, Nature (London) **508**, 500 (2014).

[8] R. Barends, A. Shabani, L. Lamata, J. Kelly, A. Mezzacapo, U. Las Heras, R. Babbush, A. G. Fowler, B. Campbell, Y. Chen *et al.*, Nature (London) **534**, 222 (2016).

[9] H. Bernien, S. Schwartz, A. Keesling, H. Levine, A. Omran, H. Pichler, S. Choi, A. S. Zibrov, M. Endres, M. Greiner, V. Vuletić, and M. D. Lukin, Nature (London) **551**, 579 (2017).

[10] B. Lekitsch, S. Weidt, A. G. Fowler, K. Mølmer, S. J. Devitt, C. Wunderlich, and W. K. Hensinger, Sci. Adv. **3**, e1601540 (2017).

[11] R. Raussendorf and H. J. Briegel, Phys. Rev. Lett. **86**, 5188 (2001).

[12] R. Raussendorf, D. E. Browne, and H. J. Briegel, Phys. Rev. A **68**, 022312 (2003).

[13] R. Raussendorf, J. Harrington, and K. Goyal, Ann. Phys. **321**, 2242 (2006).

[14] J. Eisert and H. J. Briegel, Phys. Rev. A **64**, 022306 (2001).

[15] P. Walther, K. J. Resch, T. Rudolph, E. Schenck, H. Weinfurter, V. Vedral, M. Aspelmeyer, and A. Zeilinger, Nature (London) **434**, 169 (2005).

[16] R. Prevedel, P. Walther, F. Tiefenbacher, P. Böhi, R. Kaltenbaek, T. Jennewein, and A. Zeilinger, Nature (London) **445**, 65 (2007).

[17] M. S. Tame, R. Prevedel, M. Paternostro, P. Böhi, M. S. Kim, and A. Zeilinger, Phys. Rev. Lett. **98**, 140501 (2007).

[18] H. Wang, C.-P. Yang, and F. Nori, Phys. Rev. A **81**, 052332 (2010).

[19] R. Stock and D. F. V. James, Phys. Rev. Lett. **102**, 170501 (2009).

[20] B. P. Lanyon, P. Jurcevic, M. Zwerger, C. Hempel, E. A. Martinez, W. Dür, H. J. Briegel, R. Blatt, and C. F. Roos, Phys. Rev. Lett. **111**, 210501 (2013).

[21] D. Leibfried, R. Blatt, C. Monroe, and D. Wineland, Rev. Mod. Phys. **75**, 281 (2003).

[22] R. Gerritsma, B. P. Lanyon, G. Kirchmair, F. Zähringer, C. Hempel, J. Casanova, J. J. García-Ripoll, E. Solano, R. Blatt, and C. F. Roos, Phys. Rev. Lett. **106**, 060503 (2011).

[23] M. H. Devoret, A. Wallraff, and J. M. Martinis, arXiv:cond-mat/0411174 (unpublished).

[24] A. Blais, J. Gambetta, A. Wallraff, D. I. Schuster, S. M. Girvin, M. H. Devoret, and R. J. Schoelkopf, Phys. Rev. A **75**, 032329 (2007).

[25] J. Q. You and F. Nori, Nature (London) **474**, 589 (2011).

[26] I. Buluta, S. Ashhab, and F. Nori, Rep. Prog. Phys. **74**, 104401 (2011).

[27] X. Gu, A. F. Kockum, A. Miranowicz, Y. X. Liu, and F. Nori, Phys. Rep. **718**, 1 (2017).

[28] M. Neeley, R. C. Bialczak, M. Lenander, E. Lucero, M. Mariantoni, A. D. O'Connell, D. Sank, H. Wang, M. Weides, J. Wenner, Y. Yin, T. Yamamoto, A. N. Cleland, and J. M. Martinis, Nature (London) **467**, 570 (2010).

[29] C. Song, K. Xu, W. Liu, C.-p. Yang, S.-B. Zheng, H. Deng, Q. Xie, K. Huang, Q. Guo, L. Zhang *et al.*, Phys. Rev. Lett. **119**, 180511 (2017).

[30] D. Ristè, J. G. van Leeuwen, H.-S. Ku, K. W. Lehnert, and L. DiCarlo, Phys. Rev. Lett. **109**, 050507 (2012).

[31] D. Ristè, C. C. Bultink, K. W. Lehnert, and L. DiCarlo, Phys. Rev. Lett. **109**, 240502 (2012).

[32] R. Vijay, C. Macklin, D. H. Slichter, S. J. Weber, K. W. Murch, R. Naik, A. N. Korotkov, and I. Siddiqi, Nature (London) **490**, 77 (2012).

[33] T. Tanamoto, Y.-X. Liu, S. Fujita, X. Hu, and F. Nori, Phys. Rev. Lett. **97**, 230501 (2006).

[34] J. Q. You, X.-B. Wang, T. Tanamoto, and F. Nori, Phys. Rev. A **75**, 052319 (2007).

[35] T. Tanamoto, Y.-X. Liu, X. Hu, and F. Nori, Phys. Rev. Lett. **102**, 100501 (2009).

[36] C.-W. Wu, Y. Han, X.-J. Zhong, P.-X. Chen, and C.-Z. Li, Phys. Rev. A **81**, 034301 (2010).

[37] J. M. Martinis and M. R. Geller, Phys. Rev. A **90**, 022307 (2014).

[38] R. Barends, J. Kelly, A. Megrant, D. Sank, E. Jeffrey, Y. Chen, Y. Yin, B. Chiaro, J. Mutus, C. Neill *et al.*, Phys. Rev. Lett. **111**, 080502 (2013).

[39] H. J. Briegel and R. Raussendorf, Phys. Rev. Lett. **86**, 910 (2001).

[40] D. Ristè and L. DiCarlo, arXiv:1508.01385 (unpublished).

[41] F. Albarrán-Arriagada, L. Lamata, E. Solano, G. Romero and J. C. Retamal, Phys. Rev. A **97**, 022306 (2018).

[42] A. Barenco, C. H. Bennett, R. Cleve, D. P. DiVincenzo, N. Margolus, P. Shor, T. Sleator, J. A. Smolin and H. Weinfurter, Phys. Rev. A **52**, 3457 (1995).